Hindawi
Shock and Vibration
Volume 2021, Article ID 1480264, 10 pages
https://doi.org/10.1155/2021/1480264

Research Article

A Composite Matching Layer with Anti-Reflection Characteristics for Broadband Acoustic Scattering Reduction

Shande Li,[1,2] **Xiaoxun Wu**,[1] **Jinxiu Duan**,[1] **Shuai Yuan**,[1] **Cun Wang**,[1] **Yane Ma**,[2] **and Zhifu Zhang**[1]

[1]*State Key Laboratory of Digital Manufacturing Equipment and Technology, School of Mechanical Science and Engineering, Huazhong University of Science and Technology, Wuhan 430074, China*
[2]*Hubei Institute of Specialty Vehicle, Suizhou 441300, China*

Correspondence should be addressed to Zhifu Zhang; jeff.zfzhang@foxmail.com

Received 25 June 2021; Revised 19 October 2021; Accepted 25 November 2021; Published 15 December 2021

Academic Editor: Zhuhua Tan

A composite matching layer composed of periodically arranged scatters with anti-reflection (AR) characteristics is proposed for broadband scattering reduction. The anti-reflection structure is composed of periodically arranged metal foam scatters, and it is the first attempt to be applied in the field of suppressing acoustic reflection. A complete theoretical model is developed to reveal the mechanism of scattering reduction and acoustic absorption based on effective medium theory and the transfer matrix method. The correctness and effectiveness of the theoretical model are verified by the finite element method (FEM), showing acoustic reflectance of less than 13.5% at broadband frequencies. The variation trends of reflectance are deeply investigated. The superior acoustic scattering reduction performance suggests that the matching layer possesses potential for acoustic imaging equipment and acoustic stealth.

1. Introduction

Acoustic matching layers have become the most popular subject due to the flexibility of design and application. Many scholars attempt to develop an acoustic structure to effectively suppress reflections. In optics, the anti-reflection structure has excellent performance in reducing scattering and improving the imaging quality of the lenses, but it has not been widely used in acoustics. Therefore, the anti-reflection structure composed of periodically arranged metal foam scatters is applied in the acoustic matching layer in this paper, and the acoustic reflection performance is studied. It is worth noting that this is the first attempt to apply the anti-reflection structure composed of periodically arranged scatters to acoustic matching layers for sound absorption and noise reduction.

In the past few decades, many scholars have proposed varieties of flat multilayered acoustic matching layers, and the acoustic properties were theoretically and experimentally studied [1–3]. Sharma et al. [4] investigated a soft elastic medium comprising periodic cylindrical voids attached to a steel backing, which provided further insights into the physical mechanisms associated with the system acoustic performance. Su et al. [5] conducted experimental analysis and numerical simulation on the multilayered structure composed of glass wool, rubber, and polyurethane foam. Pan and Martellotta [6] conducted a parametric study of resonant absorbers made of microperforated membranes and perforated panels to achieve sound absorption in different frequency bands through different combinations. Their research studies were more concerned with acoustic absorption in engineering. At the same time, acoustic scattering is equally important.

With the development of the acoustic absorption technique, more and more attention has been paid to anti-reflection matching layers. For years, the anti-reflection structures have been widely used in optics [7, 8] to improve image quality of the lenses. Lots of studies proved that they can also be applied to acoustics [9, 10]. Wang et al. [11] proposed a theoretical method for evaluating the noise

reduction characteristics of underwater damping materials. Xie et al. [12] intended to realize the manipulation of acoustic waves and the dissipation of acoustic energy based on the characteristics of impedance matching. They designed tapered labyrinthine acoustic metamaterials for broadband impedance matching and conducted experiments to prove the potential of the structure. Park and Lee [13] theoretically developed a one-dimensional acoustic anti-reflection device containing membranes and open tubes with negative index, which provided new directions for the study. It can be found from recent research that the impedance has a great influence on the reflectance; therefore, a precise impedance of the anti-reflection structure is required, which poses new challenges.

To precisely design the impedance of anti-reflection structures, the periodically arranged scatters, which are widely used in energy harvesting [14], wave focusing [15], and acoustic stealth [16], are introduced into the research of anti-reflection devices. Based on the antireflection coating theory, Wang et al. [17] calculated the transmission in anti-reflection devices consisting of periodically arranged scatters. Physical analysis showed that the anti-reflection device could enhance the coupling with external waves. Wu and Chen [18] introduced a multilayered anti-reflection device with periodically arranged scatters into the graded sonic crystal bending waveguide.

All studies reviewed provided important insights into the matching layers in acoustics. At present, the matching layers are difficult to dissipate energy efficiently and reduce scattering at the same time, which is an urgent problem to be solved. Anti-reflection structure can promote acoustic coupling, which can not only dissipate energy but also reduce scattering. The anti-reflection structure composed of periodically arranged scatters has only been used in acoustic imaging in previous studies. In view of that, we propose a composite matching layer with anti-reflection structure composed of periodically arranged scatters for broadband scattering reduction. This is the first attempt to apply the anti-reflection structure to the matching layer. Similar structures have not been reported yet.

2. Theoretical Model of the Composite Matching Layer

The matching layer consists of an anti-reflection structure (layers 1 and 2), a perforated plate (layer 3), and a porous layer (layer 4) from top to bottom as illustrated in Figure 1. The thickness, Young's modulus, density, and area of the m-th layer are recorded as h_m, E_m, ρ_m, and S_m, respectively.

Different from the traditional anti-reflection coating (ARC), the ARC proposed in this paper introduced the periodically arranged scatters into the field of traditional ARC. Layer 3 is a perforated plate, where the Helmholtz resonators formed by the air cavities and the holes can dissipate part of the acoustic energy, thereby reducing the acoustic scattering. There are many pores in the porous layer (layer 4), and partial vibration energy caused by acoustic waves will gradually transform into thermal energy.

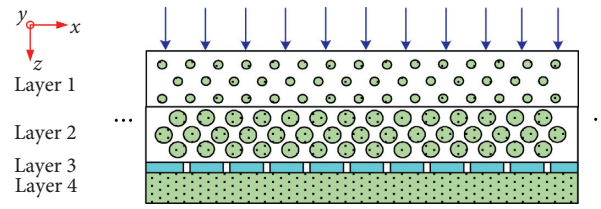

Figure 1: Cross section of the proposed matching layer.

2.1. Homogenization of Periodically Arranged Scatters. The homogenization method is applied to retrieve the effective parameters. Based on the sub-wavelength assumption, each layer can be considered as a homogeneous one with effective acoustic properties [19]. For the hexagonal arrangement of scatters in this model, the effective parameters can be expressed as [20]

$$\begin{aligned}\rho_{\text{eff}} &= \frac{\rho_a(1+ff)+\rho_b(1-ff)}{\rho_a(1-ff)+\rho_b(1+ff)}\rho_b,\\ \frac{1}{B_{\text{eff}}} &= \frac{1-ff}{B_b}+\frac{ff}{B_a},\\ c_{\text{eff}} &= \sqrt{\frac{B_{\text{eff}}}{\rho_{\text{eff}}}},\\ Z_{\text{eff}} &= \rho_{\text{eff}}\cdot c_{\text{eff}},\end{aligned} \tag{1}$$

where ff is the filling fraction, ρ, B, c and Z are mass density, bulk modulus, wave speed, and impedance, and the subscripts a, b, and eff represent the scatters, background medium, and equivalent medium, respectively.

2.2. Equivalent Parameters of Porous Materials. The Johnson–Champoux–Allard (JCA) model, which is a generalized model based on the Biot theory [21] taking the viscous effect and the thermal effect into account, can accurately describe the equivalent parameters of the porous materials in this paper. The expressions of dynamic parameters are [22]

$$\begin{aligned}\rho_e &= \frac{\alpha_\infty\rho_0}{\varphi}\left(1+\frac{\sigma\varphi}{j\omega\alpha_\infty\rho_0}\sqrt{1+\frac{4j\alpha_\infty^2\eta\rho_0\omega}{\sigma^2\Lambda^2\varphi^2}}\right),\\ B_e &= \frac{\gamma P_0/\varphi}{\gamma-\gamma-1/1+8\eta/j\Lambda\prime^2P_r\omega\rho_0\sqrt{1+j\rho_0\Lambda\prime^2P_r\omega/16\eta}},\end{aligned} \tag{2}$$

where j is an imaginary unit, ω is the angular frequency, and ρ_0, η, γ, P_0, and P_r are the mass density, the viscosity, the specific heat ratio, the equilibrium pressure, and the Prandtl constant of the air. There are five parameters associated with the porous material, and they are porosity φ, flow resistivity σ, tortuosity α_∞, viscous characteristic length Λ, and thermal characteristic length Λ'. A metal foam with $\varphi = 0.96$, $\sigma = 184269\ \text{N}\cdot\text{m}^{-4}$, $\alpha_\infty = 1.045$, $\Lambda = 3.3\times10^{-5}$ m, and $\Lambda' = 6.07\times10^{-5}$ m is selected for the study.

2.3. Theory of Anti-Reflection (AR) Structure. The basic idea of the anti-reflection structure is to insert a layer of other medium between the two mediums, whose impedance and thickness are optimally designed, so that the multiple reflected beams in the layer interfere with each other, thereby reducing or even eliminating reflection before insertion [23].

To clarify the principle of ARC, the case of oblique incidence is first discussed.

For the ARC, the impedance of layer 1 is as follows [23, 24]:

$$Z_1 = \sqrt{Z_0 \cdot Z_2}. \tag{3}$$

As described in Figure 2, the reflection coefficient of the ARC can be calculated as [25]

$$R = \left|r_1 - r_2\right|^2, \tag{4}$$

with $r_1 = Z_1 \cos\theta_i - Z_0 \cos\theta_m / Z_1 \cos\theta_i + Z_0 \cos\theta_m$ and $r_2 = Z_2 \cos\theta_m - Z_1 \cos\theta_t / Z_2 \cos\theta_m + Z_1 \cos\theta_t$.

According to Figure 2, the wave path difference can be derived as

$$\phi = 2n_1 h_1 \cos\theta_t. \tag{5}$$

When the wave path difference is an odd multiple of half wavelength and the reflection coefficients are equal, the two columns of waves can be destructive, and in this paper, acoustic waves are normally incident; therefore, the thickness of the ARC layer can be expressed as

$$h_1 = (2k+1)\lambda_0 / (4n_1)\ (k = 0, 1, 2\ldots), \tag{6}$$

where λ_0 is the wavelength.

When the impedance of the anti-reflection layer is determined, the filling fraction of layer 1 is necessary to be obtained from the equivalent impedance by solving the following equation:

$$E \cdot F f f^2 + (E \cdot B_a - D \cdot F + C \cdot E) f f + (C \cdot D - D \cdot B_a) = 0, \tag{7}$$

with $C = \rho_b \cdot B_a \cdot B_b / (Z_{\text{eff}}^2)$, $D = \rho_a + \rho_b$, $E = \rho_b - \rho_a$, and $F = B_b - B_a$, respectively.

It is worth noting that the concept of sonic crystal is introduced into the AR structure for the precise control of impedance by controlling the filling fraction of the scatters.

2.4. Transfer Matrix of the Composite Matching Layer. When acoustic waves propagate through the composite matching layer, the transfer matrix can be used to demonstrate the relationship between the outputs and the inputs, and the matrices of all component layers can be combined to form a total matrix to predict the acoustic properties [25, 26]. The transfer relation of the nonzero components $(\vec{v}, \vec{T})$, namely, vibration velocity and stress, in the layer from plane $\amalg_z$ to $\amalg_{z+H}$ is expressed as follows [27]:

$$\begin{bmatrix} v_x \\ v_z \\ T_z \\ T_x \end{bmatrix}_{z+H} = T \begin{bmatrix} v_x \\ v_z \\ T_z \\ T_x \end{bmatrix}_z = \begin{bmatrix} t_{11} & t_{12} & t_{13} & t_{14} \\ t_{21} & t_{22} & t_{23} & t_{24} \\ t_{31} & t_{32} & t_{33} & t_{34} \\ t_{41} & t_{42} & t_{43} & t_{44} \end{bmatrix} \begin{bmatrix} v_x \\ v_z \\ T_z \\ T_x \end{bmatrix}_z. \tag{8}$$

The composite matching layer with the thickness H is located between two infinite half spaces of $z < 0$ and $z > H$. The acoustic wave propagation at the interface is indicated in Figure 2, where k_i and k_r are the incident and reflected wavenumber vectors. $k_\perp$ and k_z are components of k_i decomposed in x and z directions. The transverse and longitudinal waves are separated by superscripts T and L. The wavenumbers are defined as [27]

$$\begin{aligned} \left(\overrightarrow{k_i^L}\right)^2 &= \frac{\rho\omega^2}{\lambda + 2\mu}, \\ \left(\overrightarrow{k_i^T}\right)^2 &= \frac{\rho\omega^2}{\mu}, \end{aligned} \tag{9}$$

where λ and μ are the Lamé coefficients.

Based on the wave propagation theory, Φ and Ψ indicate the propagation characteristics of longitudinal and transverse waves [27, 28]:

$$\begin{aligned} \Phi(x,z,t) &= \left(A_+^L e^{jk_z^L z} + A_-^L e^{-jk_z^L z}\right) e^{j\left(k_\perp x - \omega t\right)}, \\ \psi(x,z,t) &= \left(A_+^L e^{jk_z^L z} + A_-^T e^{-jk_z^T z}\right) e^{j\left(k_\perp x - \omega t\right)}, \end{aligned} \tag{10}$$

where A is the amplitude and the subscripts indicate the vibration direction. The vibration displacement function in x and z directions can be expressed as [28]

$$\begin{aligned} \chi(x,z,t) &= \frac{\partial\Phi}{\partial x} - \frac{\partial\Psi}{\partial z}, \\ \xi(x,z,t) &= \frac{\partial\Phi}{\partial z} + \frac{\partial\Psi}{\partial x}. \end{aligned} \tag{11}$$

To facilitate writing, variables M and N are introduced for variable substitution:

$$\begin{aligned} M^u(z) &= A_+^u e^{jk_z^u z} + A_-^u e^{-jk_z^u z}, \\ N^u(z) &= A_+^u e^{jk_z^u z} - A_-^u e^{-jk_z^u z}. \end{aligned} \tag{12}$$

The vibration speed and stress are as follows:

$$\begin{aligned} v_x &= -j\omega k_z^T N^T e^{-j\omega t}, \\ v_z &= j\omega k_z^L N^L e^{-j\omega t}, \\ T_x &= j\rho\omega^2 M^T e^{-j\omega t}, \\ T_z &= -j\rho\omega^2 M^L e^{-j\omega t}. \end{aligned} \tag{13}$$

As a result, the expression of the vibration velocity and stress of the upper interface to the lower interface can be obtained, and it is described as [28]

$$\begin{bmatrix} v_x \\ v_z \\ T_z \\ T_x \end{bmatrix}_{z+h} = A(h) \begin{bmatrix} v_x \\ v_z \\ T_z \\ T_x \end{bmatrix}_z, \tag{14}$$

with

$$A(h) = \begin{bmatrix} \cos\left(k_z^T h\right) & 0 & 0 & -j\dfrac{k_z^T \sin\left(k_z^T h\right)}{\rho\omega} \\ 0 & \cos\left(k_z^L h\right) & -j\dfrac{k_z^L \sin\left(k_z^L h\right)}{\rho\omega} & 0 \\ 0 & -j\dfrac{\rho\omega \sin\left(k_z^L h\right)}{k_z^L} & \cos\left(k_z^L h\right) & 0 \\ -j\dfrac{\rho\omega \sin\left(k_z^T h\right)}{k_z^T} & 0 & 0 & \cos\left(k_z^T h\right) \end{bmatrix}. \tag{15}$$

However, for layer 3, the stress is no longer continuous due to the presence of the intermediate hole, and the original matrix should be corrected by an amendatory matrix; it is expressed as follows [27, 28]:

$$S_3^{Am} = \begin{bmatrix} 1 & 1 & 1/S_3 & 1/S_3 \\ 1 & 1 & 1/S_3 & 1/S_3 \\ S_3 & S_3 & 1 & 1 \\ S_3 & S_3 & 1 & 1 \end{bmatrix}. \tag{16}$$

Hence, the transfer matrix of layer 3 can be written as

$$A_3^{\text{hom}} = S_3^{Am} \circ A_3. \tag{17}$$

Therefore, the transfer matrix of the stress form can be expressed as [27, 28]

$$T = S_e \circ \left(A_4(h_4) \times A_3^{\text{hom}}(h_3) \times A_2(h_2) \times A_1(h_1)\right), \tag{18}$$

with

$$S_e = \begin{bmatrix} 1 & 1 & S_0 & S_0 \\ 1 & 1 & S_0 & S_0 \\ 1/S_4 & 1/S_4 & 1 & 1 \\ 1/S_4 & 1/S_4 & 1 & 1 \end{bmatrix}. \tag{19}$$

What calls for special attention is that the velocity of the transverse wave is 0. The present matrix can be eventually written as the following one by deducing T_x [26, 28].

$$\begin{bmatrix} z \\ v \\ z \\ T \end{bmatrix}_{z=H} = Q \begin{bmatrix} z \\ v \\ z \\ T \end{bmatrix}_{z=0}, \tag{20}$$

with

$$Q = \begin{bmatrix} t_{22} - \dfrac{t_{21}{}_t^{42}}{t_{41}} & t_{23} - \dfrac{t_{21}{}_t^{43}}{T_{41}} \\ t_{32} - \dfrac{t_{31}{}_t^{42}}{t_{41}} & t_{33} - \dfrac{t_{31}{}_t^{43}}{t_{41}} \end{bmatrix}. \tag{21}$$

When the composite matching layer is placed in two semi-infinite spaces with impedances of Z_0 and Z_5 at the incident and transmitted ends, respectively, the following formula can be obtained [26, 28]:

$$\tau \begin{bmatrix} 1 \\ Z_5 \end{bmatrix} = \begin{bmatrix} q_{11} & q_{12} \\ q_{21} & q_{22} \end{bmatrix} \begin{bmatrix} 1+R \\ Z_0(1+R) \end{bmatrix}. \tag{22}$$

Transmission coefficient τ and reflection coefficient R can be obtained by solving equation (22).

$$\begin{aligned} \tau &= -\frac{2(q_{12}q_{21} - q_{11}q_{22})Z_0}{q_{21} - Z_0 q_{22} - (q_{11} - Z_0 q_{12})Z_5}, \\ R &= -\frac{q_{21} + Z_0 q_{22} - (q_{11} + Z_0 q_{12})Z_5}{q_{21} - Z_0 q_{22} - (q_{11} - Z_0 q_{12})Z_5}. \end{aligned} \tag{23}$$

3. Foundation and Validation of Theoretical Analysis

3.1. Parameter Properties and Preconditions for Model Application. For the composite matching layer, plane waves with amplitudes $p_i = 1$ Pa normally enters into it, and the medium is air with density $\rho_0 = 1.21\ \text{kg/m}^3$ and acoustic velocity $c_0 = 344$ m/s, respectively. The scatters in layer 1 and layer 2 are made of the same porous material as layer 4, and the matrix material is air. Layer 3 is made of isobutylene isoprene rubber (IIR), and $\rho_3 = 1005\ \text{kg/m}^3$,

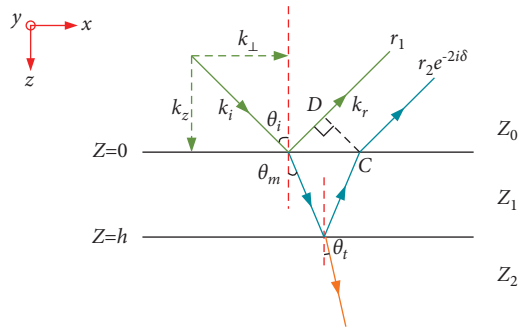

Figure 2: Acoustic wave propagation in anti-reflection structure.

$E_3 = 42.4$ MPa, and $v_3 = 0.47$. The thickness of the entire composite matching layer is 53 mm.

For layer 1 and layer 2, the derivation of the homogenization method is based on the sub-wavelength assumption. Therefore, the precondition for application is that $\lambda > 4a$, and hence the upper limit frequency is determined by

$$f_{\max} = \frac{c}{4a}. \tag{24}$$

In this paper, the lattice constant $a = 0.0085$ m, and thus $f_{\max} = 10118$ Hz. Therefore, we focus on the bandwidth of 200 Hz–10000 Hz for study.

3.2. Model Validation. In this section, simulation analysis is performed by the finite element method to verify the reliability of the model. The basic idea of this method is to discretize the structure and use a limited number of units to express the composite matching layer. The units are connected to each other through a limited number of nodes, then solved according to the deformation coordination conditions, and then verified with the theoretical method in this paper. The geometric model is shown in Figure 3. The background pressure field is applied to the air field, which is incident perpendicularly. The part with the width W is truncated, and the left and right boundaries are set as periodic Floquet boundaries to represent the infinitely large cladding layer. At the top of the air domain, the perfect matching layer (PML) represents the semi-infinite air domain.

The reflectance of the theoretical model and the simulation model with the same parameters is predicted by the plane wave. The comparison between the acoustic reflectance curves is displayed in Figure 4. The reflectance of the theoretical solution and the simulated solution is perfectly coincident, which proves the correctness of the proposed theoretical model.

It can be seen from Figure 4 that when the frequency approaches 0, the structural reflectance tends to 1. A possible explanation is that at low frequencies, the wavelength is much larger than the size of the matching layer, the sound waves are diffracted, and they directly strike the rigid wall, resulting in high reflectance. At 200–800 Hz, the reflectance decreases rapidly and the reflectance is less than 13.5% at 800–10000 Hz, showing that the matching layer can make the incident acoustic waves coupled into the scatters as efficiently as possible, thereby reducing reflection. To be more obvious, several representative frequency points have been extracted. It is found that at 900 Hz, 3000 Hz, and 7000 Hz, the reflectance is 10%, 11%, and 6.6%, respectively. The corresponding scattered field contours of the matching layer obtained by theoretical calculation are shown in Figure 5, which indicate that the proposed matching layer has an excellent effect of suppressing scattering.

4. Parametric Research and Discussion

To further reveal the acoustic characteristics of the composite matching layer, several configuration parameters are discussed, covering structural parameters of every layer and material parameters. These parameters can change the impedance of the matching layer, which in turn affects the mechanism of absorption and reflection.

4.1. Effects of ARC. The periodically arranged scatters are introduced into the ARC, which allows precise control of the impedance and flexible design. The parameters of ARC are indispensable in changing the impedance, thus affecting the mechanism of energy transfer and dissipation.

4.1.1. Variation Tendency with the Thickness. When the thickness is properly designed, the ARC can be adapted to different applications. From Figure 6(a), we can see that as the thickness of layer 1 gradually increases from 0.85 to 2.55 cm, the reflectance is significantly smaller at 800–3800 Hz and 7000–10000 Hz. At 800–3800 Hz, the valley of the reflection curve drops slightly; at 7000–10000 Hz, the curves of $h_1 = 1.7$ cm and $h_1 = 2.55$ cm are almost coincident and significantly lower than those of $h_1 = 0.85$ cm. It is apparent from Figure 6(b) that as the thickness of layer 2 increases, the reflectance curve moves toward low frequencies and the first valley has a significant change.

The decrease in reflection coefficients is due to the increase in the amount of porous material available to absorb energy as the thickness increases. As the acoustic wave transmission path becomes longer, the absorption wavelength of the composite matching layer also increases, so the valley shifts to the low frequency. Therefore, the thickness of the ARC can be adjusted according to different occasions to eliminate the scattered waves.

4.1.2. Change Regulations of Lattice Constant. Based on the single variable principle, different values for the lattice constant a = (6.5, 7.5, 8.5) mm are discussed. In Figure 7, comparing the matching layers with different lattice constants, it is found that a reflection increase occurs in the middle frequency range, and the average reflectance in the whole studied frequency range is obviously reduced as the lattice constant becomes larger. At the same time, the reflection curve moves to low frequencies, showing a better performance at low frequencies.

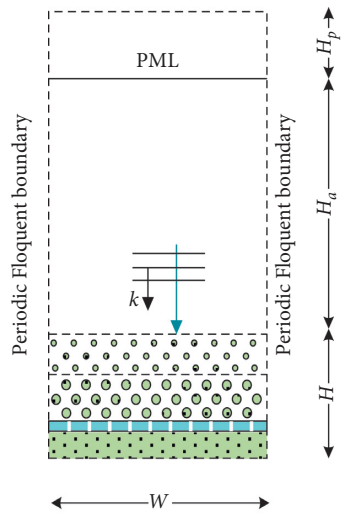

Figure 3: Geometric schematic of the finite element model of the matching layer.

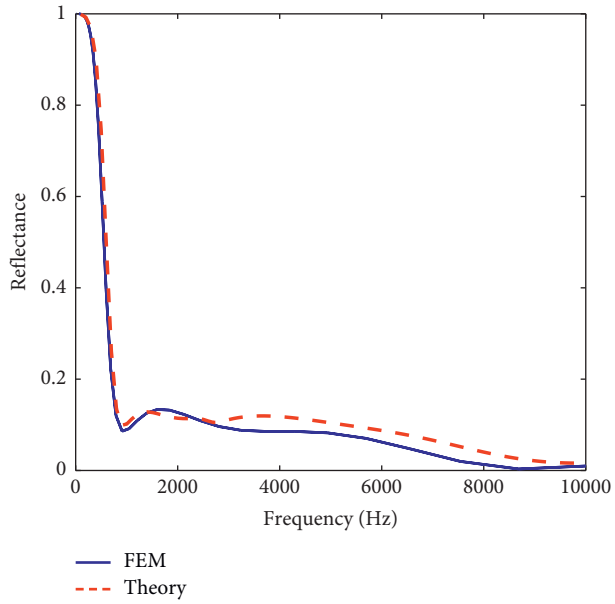

Figure 4: Comparison of theoretical calculations and finite element simulation results.

The reason is that the filling fraction decreases with the increase of the lattice constant, which makes the impedance transition smoother, thus enhancing the coupling of acoustic waves and scatters and promoting energy consumption.

4.2. Effects of Perforated Plate Parameters. To study the influence of the perforated plate parameters on absorption, the perforation rate $\varepsilon = (5\%, 15\%, 25\%)$ and the thickness $h_3 = (1, 2, 3)$ mm are discussed in detail. It is obvious in Figure 8(a) that as the perforation rate increases, the first valley moves toward high frequencies, and the reflectance of the low frequencies decreases. The curves in Figure 8(b) showed that the thickness of layer 3 only influences the acoustic reflectance at 1000–2000 Hz. The second valley shifts toward the low frequencies as the perforation rate increases.

The reason is that the variation of perforation rate and the thickness directly changes the sizes of the Helmholtz resonators and affects the energy dissipation mode of the cavity resonance.

4.3. Effects of Parameters of Porous Material. It is widely recognized by scholars that the acoustic absorption performance of porous materials can be determined by five parameters and the influence of porosity and flow resistivity is obvious. The cases when $\varphi = (0.90, 0.93, 0.96)$ are discussed, and the results are displayed in Figure 9(a). As the porosity is increased from 0.90 to 0.96, the acoustic reflection coefficients drop at all frequencies. The reason is that as the porosity of the porous material increases, the number of pores inside the porous material increases, and the

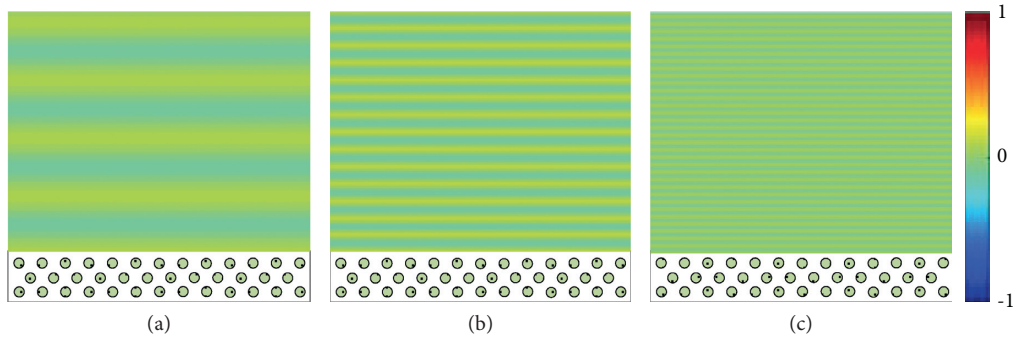

Figure 5: Scattered field contours obtained by theoretical calculation at different frequencies. (a) $f_1 = 900$ Hz. (b) $f_2 = 3000$ Hz. (c) $f_3 = 7000$ Hz.

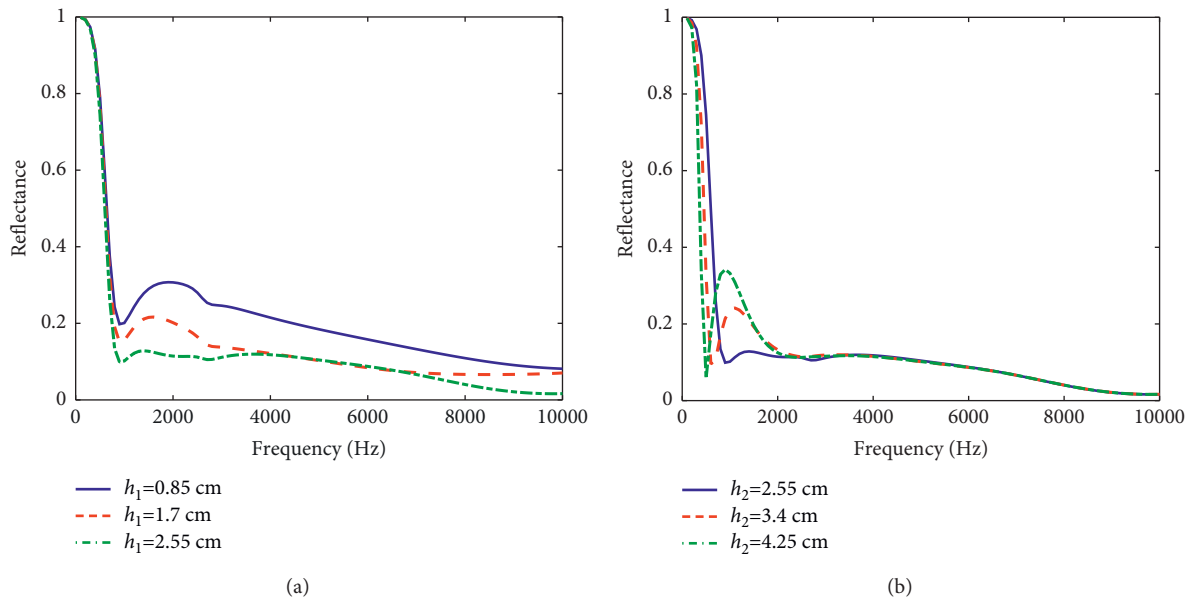

Figure 6: Acoustic reflection curves with different ARC parameters. (a) Thickness of layer 1. (b) Thickness of layer 2.

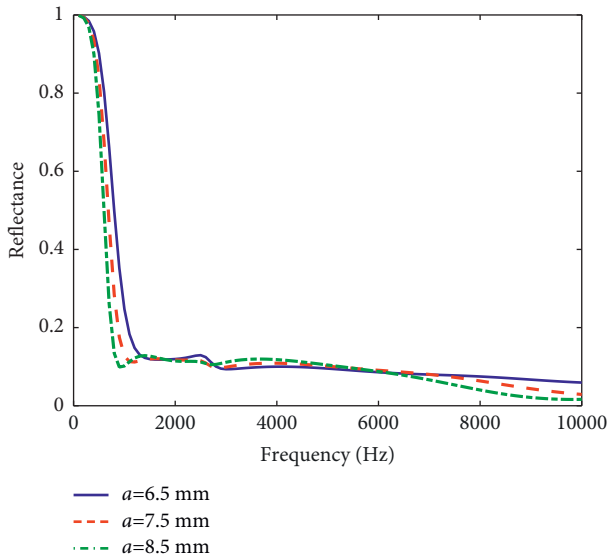

Figure 7: Acoustic reflection curves with different lattice constants.

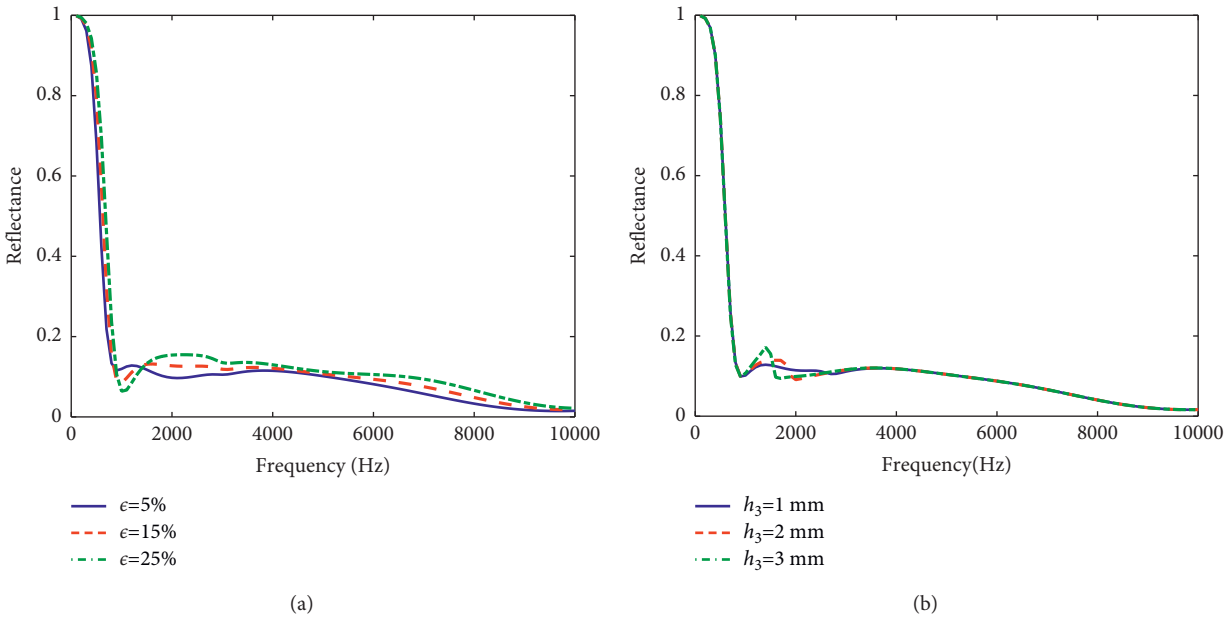

Figure 8: Acoustic reflection curves with different parameters of the perforated layer. (a) The perforation rate. (b) The thickness of layer 3.

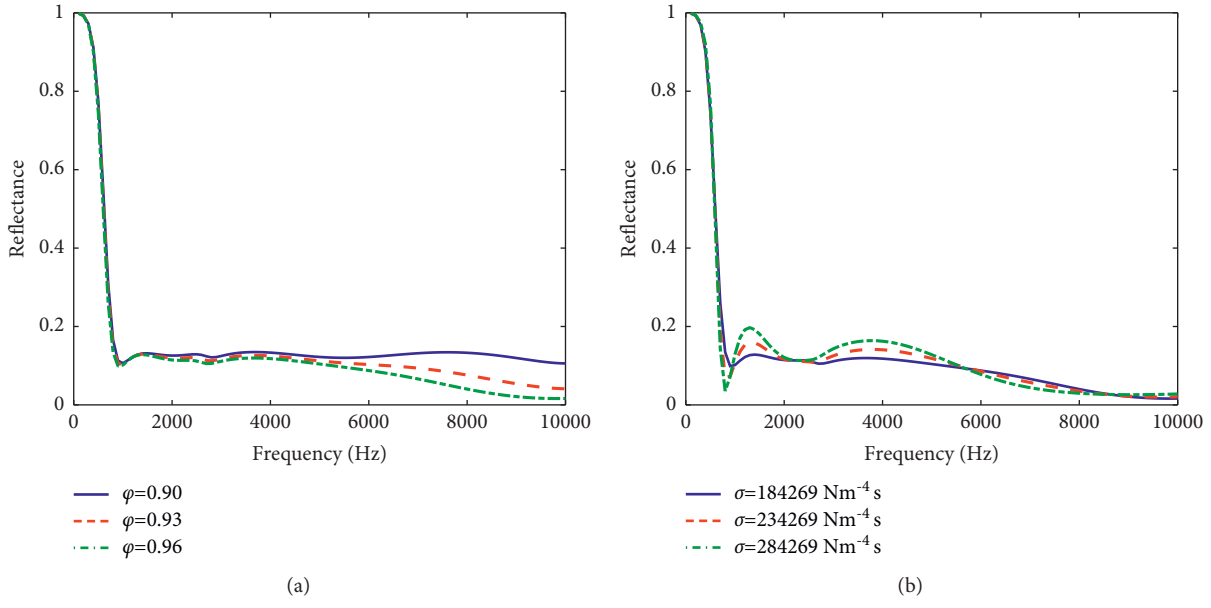

Figure 9: Acoustic reflection curves with different parameters of the porous layer. (a) The porosity. (b) The flow resistivity.

acoustic waves can better enter the material along the pores and cause air vibration, thereby more effectively absorbing energy and reducing acoustic reflection.

Flow resistivity affects the efficiency of acoustic energy loss in porous materials due to friction and viscosity. Figure 9(b) shows the reflection curves with different flow resistivity $\sigma = (134269,\ 184269,\ 234269)\ \mathrm{N{\cdot}m^{-4}s}$, respectively. It can be seen that when the flow resistivity increases, the reflectance at high frequencies becomes lower, but when the flow resistivity is too large, other properties of the structure will also be affected. Therefore, the appropriate flow resistivity can achieve the best acoustic performance of the structure.

5. Conclusions

In summary, this paper proposes a composite matching layer with excellent acoustic performance at broadband frequencies. The composite matching layer includes a perforated plate, a porous layer, and an anti-reflection structure.

The anti-reflection structure includes periodically arranged metal foam scatters, and it is the first attempt to be applied in the field of suppressing acoustic reflection. Based on the homogenization theory, anti-reflection theory, and transfer matrix method, a complete two-dimensional theoretical model is developed. The correctness and effectiveness of the theoretical model are verified by simulation analysis. At 200–800 Hz, the reflectance decreases rapidly and the reflectance is less than 13.5% at 800–10000 Hz, showing that the matching layer can make the incident acoustic waves coupled into the scatters as efficiently as possible, thereby reducing reflection. The theoretical solution of the model shows that the acoustic scattering can be reduced at broadband frequencies. The variation trends of reflectance are investigated to reveal the mechanism of scattering reduction and acoustic absorption. All the results show that the composite matching layer can effectively reduce the acoustic scattering by enhancing the coupling of acoustic waves. Hence, the composite matching layer proposed provides a promising future for acoustic imaging equipment and acoustic stealth.

Data Availability

The data used to support the findings of this study are included within the article.

Conflicts of Interest

The authors declare that there are no conflicts of interest regarding the publication of this paper.

Acknowledgments

This study was supported by the Natural Science Foundation of Hubei Province (grant no. 2020CFB510) and the National Natural Science Foundation of China (grant no. 51575201).

References

[1] W. T. Thomson, "Transmission of elastic waves through a stratified solid medium," *Journal of Applied Physics*, vol. 21, no. 2, pp. 89–93, 1950.

[2] E. Meyer, K. Brendel, and K. Tamm, "Pulsation oscillations of cavities in rubber," *Journal of the Acoustical Society of America*, vol. 30, no. 12, pp. 1116–1124, 1958.

[3] S. M. Ivansson, "Sound absorption by viscoelastic coatings with periodically distributed cavities," *Journal of the Acoustical Society of America*, vol. 119, no. 6, pp. 3558–3567, 2006.

[4] G. S. Sharma, A. Skvortsov, I. Macgillivray, and N. Kessissoglou, "Acoustic performance of gratings of cylindrical voids in a soft elastic medium with a steel backing," *Journal of the Acoustical Society of America*, vol. 141, no. 6, pp. 4694–4704, 2017.

[5] J. Su, L. Zheng, and Z. Deng, "Study on acoustic properties at normal incidence of three-multilayer composite made of glass wool, glue and polyurethane foam," *Applied Acoustics*, vol. 156, pp. 319–326, 2019.

[6] L. Pan and F. Martellotta, "A parametric study of the acoustic performance of resonant absorbers made of micro-perforated membranes and perforated panels," *Applied Sciences*, vol. 10, no. 5, p. 1581, 2020.

[7] S. Walheim, E. Schäffer, J. Mlynek, and U. Steiner, "Nanophase-separated polymer films as high-performance antireflection coatings," *Science*, vol. 283, no. 5401, pp. 520–522, 1999.

[8] D. J. Aiken, "High performance anti-reflection coatings for broadband multi-junction solar cells," *Solar Energy Materials and Solar Cells*, vol. 64, no. 4, pp. 393–404, 2000.

[9] J. Kushibiki, T. Sannomiya, and N. Chubachi, "Performance of sputtered SiO2 film as acoustic antireflection coating at sapphire/water interface," *Electronics Letters*, vol. 16, no. 19, pp. 737-738, 1980.

[10] R. D. Corsaro, J. F. Covey, R. M. Young, and G. Spryn, "Acoustic coatings for water-filled tanks," *ACS Symposium Series*, vol. 424, pp. 208–228, 1990.

[11] C. N. Wang, C. C. Tse, and S. K. Chen, "On analysis of passive underwater acoustic damping materials," *Journal of the Chinese Institute of Engineers*, vol. 30, no. 2, pp. 251–257, 2007.

[12] Y. Xie, A. Konneker, and B. I. Popa, "Tapered labyrinthine acoustic metamaterials for broadband impedance matching," *Applied Physics Letters*, vol. 103, no. 20, 2013.

[13] C. M. Park and S. H. Lee, "Zero-reflection acoustic metamaterial with a negative refractive index," *Scientific Reports*, vol. 9, no. 1, p. 3372, 2019.

[14] S. Tol, F. L. Degertekin, and A. Erturk, "Gradient-index phononic crystal lens-based enhancement of elastic wave energy harvesting," *Applied Physics Letters*, vol. 109, no. 6, 2016.

[15] A. Zareei, A. Darabi, M. J. Leamy, and M.-R. Alam, "Continuous profile flexural GRIN lens: focusing and harvesting flexural waves," *Applied Physics Letters*, vol. 112, no. 2, p. 023901, 2018.

[16] C. Wang, W. G. Zheng, and Q. B. Huang, "Acoustic absorption characteristics of new underwater omnidirectional absorber," *Chinese Physics Letters*, vol. 36, no. 4, 2019.

[17] Y. Wang, K. Deng, S. Xu, C. Qiu, H. Yang, and Z. Liu, "Applications of antireflection coatings in sonic crystal-based acoustic devices," *Physics Letters A*, vol. 375, no. 10, pp. 1348–1351, 2011.

[18] L.-Y. Wu and L.-W. Chen, "Enhancing transmission efficiency of bending waveguide based on graded sonic crystals using antireflection structures," *Applied Physics A*, vol. 107, no. 3, pp. 743–748, 2012.

[19] Y. Jin, B. Djafari-Rouhani, and D. Torrent, "Gradient index phononic crystals and metamaterials," *Nanophotonics*, vol. 8, no. 5, pp. 685–701, 2019.

[20] A. Climente Alfonso, *Refractive Devices for Acoustical and Flexural Waves*, PhD Thesis, Universitat Politècnica de València, Valencia,Spain, 2015.

[21] M. A. Biot, "Theory of propagation of elastic waves in a fluid-saturated porous solid. II. Higher frequency range," *Journal of the Acoustical Society of America*, vol. 28, no. 2, pp. 179–191, 1956.

[22] Y. Fang, X. Zhang, and J. Zhou, "Acoustic porous metasurface for excellent sound absorption based on wave manipulation," *Journal of Sound and Vibration*, vol. 434, pp. 273–283, 2018.

[23] H. A. Macleod, *Thin-film Optical Filters*, CRC Press, Boca Raton, Florida, 2017.

[24] J. F. Tang, P. F. Gu, and X. Liu, *Modern Optical Thin Film Technology*, Zhejiang University Press, Hangzhou, China, 2006, in Chinese.

[25] C.-M. Lee and Y. Xu, "A modified transfer matrix method for prediction of transmission loss of multilayer acoustic

materials," *Journal of Sound and Vibration*, vol. 326, no. 1-2, pp. 290–301, 2009.

[26] A. Morro and G. Caviglia, "Wave propagation in a stratified layer via the matricant," *Communications in Applied and Industrial Mathematics*, vol. 2, no. 1, p. 367, 2011.

[27] P. Cervenka and P. Challande, "A new efficient algorithm to compute the exact reflection and transmission factors for plane waves in layered absorbing media (liquids and solids)," *Journal of the Acoustical Society of America*, vol. 89, no. 4, pp. 1579–1589, 1991.

[28] Z. Zhang, Y. Huang, and Q. Huang, "Low-frequency broadband absorption of underwater composite anechoic coating with periodic subwavelength arrays of shunted piezoelectric patches," *Composite Structures*, vol. 216, pp. 449–463, 2019.